

## Central Lancashire Online Knowledge (CLOK)

|          |   |
|----------|---|
| Title    | Beta Dips in the Gaia Era: Simulation Predictions of the Galactic Velocity Anisotropy Parameter ( $\beta$ ) for Stellar Halos   |
| Type     | Article   |
| URL      | <a href="https://clock.uclan.ac.uk/22887/">https://clock.uclan.ac.uk/22887/</a>   |
| DOI      | <a href="https://doi.org/10.3847/1538-4357/aaa0d6">https://doi.org/10.3847/1538-4357/aaa0d6</a>   |
| Date     | 2018  |
| Citation | Loebman, Sarah R., Valluri, Monica, Hattori, Kohei, Debattista, Victor P, Bell, Eric F., Stinson, Gregory Stewart, Christensen, Charlotte R., Brooks, Alyson, Quinn, Thomas R. et al (2018) Beta Dips in the Gaia Era: Simulation Predictions of the Galactic Velocity Anisotropy Parameter ( $\beta$ ) for Stellar Halos. The Astrophysical Journal, 853 (2). p. 196. ISSN 0004-637X |
| Creators | Loebman, Sarah R., Valluri, Monica, Hattori, Kohei, Debattista, Victor P, Bell, Eric F., Stinson, Gregory Stewart, Christensen, Charlotte R., Brooks, Alyson, Quinn, Thomas R. and Governato, Fabio   |

It is advisable to refer to the publisher's version if you intend to cite from the work.  
<https://doi.org/10.3847/1538-4357/aaa0d6>

For information about Research at UCLan please go to <http://www.uclan.ac.uk/research/>

All outputs in CLOK are protected by Intellectual Property Rights law, including Copyright law. Copyright, IPR and Moral Rights for the works on this site are retained by the individual authors and/or other copyright owners. Terms and conditions for use of this material are defined in the <http://clock.uclan.ac.uk/policies/>



# Beta Dips in the *Gaia* Era: Simulation Predictions of the Galactic Velocity Anisotropy Parameter ( $\beta$ ) for Stellar Halos

Sarah R. Loebman<sup>1,2,8,9</sup> , Monica Valluri<sup>1</sup> , Kohei Hattori<sup>1</sup> , Victor P. Debattista<sup>3</sup> , Eric F. Bell<sup>1</sup> , Greg Stinson<sup>4</sup>,

Charlotte R. Christensen<sup>5</sup> , Alyson Brooks<sup>6</sup> , Thomas R. Quinn<sup>7</sup>, and Fabio Governato<sup>7</sup>

<sup>1</sup> Department of Astronomy, University of Michigan, 1085 South University Avenue, Ann Arbor, MI 48109-1107, USA

<sup>2</sup> Department of Physics, University of California, Davis, 1 Shields Avenue, Davis, CA 95616, USA; [srloebman@ucdavis.edu](mailto:srloebman@ucdavis.edu)

<sup>3</sup> Jeremiah Horrocks Institute, University of Central Lancashire, Preston PR1 2HE, UK

<sup>4</sup> Max-Planck-Institut für Astronomie, Heidelberg, Germany

<sup>5</sup> Physics Department, Grinnell College, Grinnell, IA, USA

<sup>6</sup> Department of Physics & Astronomy, Rutgers University, New Brunswick, NJ, USA

<sup>7</sup> Astronomy Department, University of Washington, Seattle, WA, USA

Received 2017 April 5; revised 2017 November 17; accepted 2017 December 8; published 2018 February 5

## Abstract

The velocity anisotropy parameter,  $\beta$ , is a measure of the kinematic state of orbits in the stellar halo, which holds promise for constraining the merger history of the Milky Way (MW). We determine global trends for  $\beta$  as a function of radius from three suites of simulations, including accretion-only and cosmological hydrodynamic simulations. We find that the two types of simulations are consistent and predict strong radial anisotropy ( $\langle\beta\rangle \sim 0.7$ ) for Galactocentric radii greater than 10 kpc. Previous observations of  $\beta$  for the MW’s stellar halo claim a detection of an isotropic or tangential “dip” at  $r \sim 20$  kpc. Using the  $N$ -body+SPH simulations, we investigate the temporal persistence, population origin, and severity of “dips” in  $\beta$ . We find that dips in the in situ stellar halo are long-lived, while dips in the accreted stellar halo are short-lived and tied to the recent accretion of satellite material. We also find that a major merger as early as  $z \sim 1$  can result in a present-day low (isotropic to tangential) value of  $\beta$  over a broad range of radii and angles. While all of these mechanisms are plausible drivers for the  $\beta$  dip observed in the MW, each mechanism in the simulations has a unique metallicity signature associated with it, implying that future spectroscopic surveys could distinguish between them. Since an accurate knowledge of  $\beta(r)$  is required for measuring the mass of the MW halo, we note that significant transient dips in  $\beta$  could cause an overestimate of the halo’s mass when using spherical Jeans equation modeling.

**Key words:** Galaxy: abundances – Galaxy: evolution – Galaxy: formation – Galaxy: halo – Galaxy: kinematics and dynamics – Galaxy: structure

## 1. Introduction

It is widely assumed that the kinematic state of the stellar halo can be used to constrain the Milky Way’s (MW) formation history (Eggen et al. 1962; Johnston et al. 2008) and mass distribution (Xue et al. 2008; Gnedin et al. 2010; Deason et al. 2012). As a result, a considerable effort has been expended in measuring the stellar halo’s kinematic moments (e.g., Xue et al. 2008; Bond et al. 2010; Cunningham et al. 2016). Recently, emphasis has been placed on the measurement of the velocity anisotropy parameter ( $\beta$ ), the ratio of tangential to radial random motion, which is expected to be positive from simple numerical experiments on halo formation (Binney & Tremaine 2008). However, measurements of  $\beta$  in the MW have suggested that it is negative within  $15 \lesssim R/\text{kpc} \lesssim 25$  (see Kafle et al. 2012, King et al. 2015, but see Deason et al. 2013b, Cunningham et al. 2016 for alternative values), leading to speculation that the exact merger and dissipation history of the stellar halo could strongly affect its velocity anisotropy profile (Deason et al. 2013a, 2013b). In spite of these recent efforts to infer the MW’s accretion history from measurements of the density profile and  $\beta$ , there have been no systematic studies of how  $\beta$  varies with radius in realistic cosmological hydrodynamic simulations that demonstrate that  $\beta$  is in fact a tracer of assembly history.

First introduced by Binney (1980) to characterize the orbital structure of a spherical system,  $\beta$  is most commonly used in spherical Jeans equation modeling to recover the mass distribution of galactic systems. In a Galactocentric spherical coordinate system ( $r, \theta, \phi$ ), corresponding to radial distance, polar angle, and azimuthal angle, we define  $\beta$  as

$$\beta(r) = 1 - \frac{\sigma_\theta(r)^2 + \sigma_\phi(r)^2}{2\sigma_r(r)^2}, \quad (1)$$

where  $\sigma_\theta, \sigma_\phi, \sigma_r$  are the velocity dispersions in spherical coordinates. In a system in which  $\beta = 1$ , all stars are on radial orbits plunging in and out of the galactic center, while in a system with  $\beta = -\infty$ , all orbits are circular. A system with an isotropic velocity distribution ( $\sigma_\theta = \sigma_\phi = \sigma_r$ ) has  $\beta = 0$ .

Models of galaxy formation generally imply that  $\beta$  increases with radius, corresponding to nearly isotropic near the center and radially biased in the outskirts (see Section 4.10.3 of Binney & Tremaine 2008, and references therein; Debattista et al. 2008). This trend has been shown in both cosmological pure  $N$ -body simulations (see Figure 10 of Diemand et al. 2005) and in cosmological  $N$ -body+SPH simulations (see Figure 5 of Abadi et al. 2006; Sales et al. 2007). Analyzing the  $z = 0$  snapshot of the high-resolution MW-like simulation Eris, Rashkov et al. (2013) also found  $\beta$  to be increasingly radially biased with distance, transitioning to purely radial stellar orbits beyond 100 kpc (see Section 4 and Figure 2 of Rashkov et al. 2013). Notably, Eris shows a “dip”

<sup>8</sup> Michigan Society of Fellows.

<sup>9</sup> Hubble Fellow.

in  $\beta$  at  $r \sim 70$  kpc, where  $\beta$  drops from  $\sim 0.75$  to  $0.5$  over a narrow range of radii, which coincides with recently accreted substructure (see Figure 3 of Rashkov et al. 2013). This hints that fluctuations in the value of  $\beta$  are possible in simulations, but does not speak directly to their duration, intensity, or frequency of occurrence. Recently, using orbital integration analysis, Bird & Flynn (2015) considered the duration of low values in  $\beta$  and found them to be short-lived (persisting a few tens of millions of years) and unconnected to the galactic density profile. Motivated by this analysis, we look at the time evolution of  $\beta$  simulated in a full cosmological context, to understand what, if any, predictive power  $\beta$  holds for constraining the formation history of the MW.

From an observational perspective,  $\beta$  is hard to measure and somewhat sensitive to small number statistics. For MW halo stars, the form of the  $\beta$ -profile measured also depends on the modeling method employed. Assuming the MW is well described by a truncated, flat rotation curve, it is possible to derive the velocity anisotropy profile from 4D data (Galactocentric radius, on-sky position, and line-of-sight velocity) using an action-based distribution function method (see, for instance, Wilkinson & Evans 1999; Deason et al. 2012). Recently, Williams & Evans (2015) constrained such a model using the blue horizontal branch catalog of Xue et al. (2011). Their best fit result for  $\beta(r)$  rises appreciably more gradually than  $\beta(r)$  from  $N$ -body simulations (see Figure 8 and Section 5.3 of Williams & Evans 2015 for further details).

In contrast, measurements of  $\beta$  for halo stars within the solar cylinder based on full 6D phase-space data find  $\beta$  to be strongly radially biased. For example, Chiba & Yoshii (1998) analyzed the kinematics of nearby stars falling within  $\sim 2$  kpc from the Sun. They leveraged proper motion (and parallax for a handful of stars) from the *Hipparcos* satellite and the photometric distance, line-of-sight velocity, and  $[\text{Fe}/\text{H}]$  from ground-based telescopes. Using 124 stars with  $[\text{Fe}/\text{H}] < -1.6$ , Chiba & Yoshii (1998) found velocity dispersions  $(\sigma_r, \sigma_\phi, \sigma_\theta) \simeq (\sigma_U, \sigma_V, \sigma_W) = (161 \pm 10, 115 \pm 7, 108 \pm 7) \text{ km s}^{-1}$ , corresponding to  $\beta = 0.52 \pm 0.07$ . Sampling a larger volume (within 5 kpc of the Sun), Smith et al. (2009) found  $\beta = 0.69 \pm 0.01$ . This value was determined using a catalog of  $\sim 1700$  halo subdwarfs selected using a reduced proper-motion diagram applied to data from Stripe 82 of the Sloan Digital Sky Survey (SDSS). Combined with radial velocities from SDSS spectra and distances from the photometric parallax relation (with uncertainty of  $\sim 10\%$ ), Smith et al. (2009) found  $(\sigma_r, \sigma_\phi, \sigma_\theta) = (143 \pm 2, 82 \pm 2, 77 \pm 2) \text{ km s}^{-1}$ . Sampling a slightly larger footprint still ( $r < 10$  kpc), pointed toward the northern Galactic cap, Bond et al. (2010) found a similar value,  $\beta \sim 0.67$ . This was determined using proper motions of a large sample of main-sequence SDSS stars from Munn et al. (2004), resulting in  $(\sigma_r, \sigma_\phi, \sigma_\theta) \sim (141, 85, 75) \text{ km s}^{-1}$ .

Beyond  $r \sim 10$  kpc, it has been extremely difficult to obtain full 6D information for a robust sample of halo stars. Since 2014, the HALO7D project (Cunningham et al. 2015) has worked to obtain accurate proper motions measured by the *Hubble Space Telescope* and very deep Keck DEIMOS spectroscopy of  $\sim 100$  main-sequence turn-off stars in the MW with the goal of assessing  $\beta$  at large radii. Analysis of 13 HALO7D stars lying within  $18 < r/\text{kpc} < 32$  yields  $\beta = -0.3_{-0.9}^{+0.4}$  (Cunningham et al. 2016). This value is consistent with isotropy and lower than the solar neighborhood  $\beta$  measurements by  $2\sigma$ . This value is also substantially lower

than model predictions of radially biased values; however, model predictions in the literature were generated in the limit that there was no satellite substructure present. Cunningham et al. (2016) note that two stars from this sample are likely members of a known substructure (TriAnd). If they exclude these stars from their analysis, they find  $\beta = 0.1_{-1.0}^{+0.4}$ , which is still formally lower than solar neighborhood measurements but just outside the  $1\sigma$  limit.

There is a robust and interesting discussion in the literature of the value of  $\beta$  beyond  $r \sim 20$  kpc based upon 4D phase-space information for thousands of blue horizontal branch stars (Sirko et al. 2004; Deason et al. 2012; Kafle et al. 2012; King et al. 2015) and 5D phase-space for a small number of halo stars (Deason et al. 2013b). Wildly divergent values for  $\beta$  have been obtained; based upon these studies, it is plausible that  $\beta$  remains radially anisotropic (Deason et al. 2012), that  $\beta$  “dips,” falling from a radial value of  $\beta \sim 0.5$ – $0.7$  at  $r < 20$  kpc to an isotropic  $\beta \sim 0$  (Sirko et al. 2004; Deason et al. 2013b), or that  $\beta$  is strongly tangentially biased, with  $\beta < -1.5$  (Kafle et al. 2012; King et al. 2015) at  $r \sim 20$ – $25$  kpc. Deason et al. (2013b) speculate that this dip could be associated with a large, shell-type structure that is a remnant of an accretion event at  $r \sim 25$  kpc; however, Johnston et al. (2008) find shell-type structures to be typically associated with stars on radial orbits at apogalactic passage.

In a companion paper (Hattori et al. 2017), we consider the impact of using 4D data instead of full 6D data to estimate  $\beta$ . We find that  $\beta$  is systematically underestimated beyond a certain radius ( $r \sim 15$  kpc for the currently available sample size). As  $r$  increases, the line-of-sight velocity approaches the Galactocentric radial velocity. This makes it difficult to extract information about the tangential velocity distribution (and hence  $\beta$ ) from the line-of-sight velocity distribution alone. The limitation of the line-of-sight velocities in recovering the velocity anisotropy was first explored in Hattori et al. (2013) and is supported by Wang et al. (2015), who find that if proper motions are not available, it is difficult to obtain robust constraints on  $\beta$ . Thus for the remainder of this paper, we will focus on  $\beta$  derived from 6D phase-space information.

We are optimistic that upcoming *Gaia* data will fill in the gaps and tighten constraints on  $\beta(r)$  for the MW (Gaia Collaboration et al. 2016). For example, with a *Gaia* sample of 2000 blue horizontal branch stars within  $15 < r/\text{kpc} < 30$  (expected distance error  $< 5\%$ ), we anticipate that a  $\beta$  dip from  $0.5$  to  $0.0$  is recoverable with an error on  $\beta < 0.2$  (see Appendix for further details). With this sensitivity in mind, in this paper, we consider what high-resolution MW-like simulations predict for  $\beta(r)$ . We aim to assemble a comprehensive set of predictions for  $\beta(r)$  for observers to reference and challenge in the coming years. In Section 2, we discuss the setup of the three suites of simulations we use. In Section 3, we present average trends in  $\beta(r)$ ; we find that all three suites are consistent and predict a monotonically increasing value of  $\beta$  that is radially biased, and  $\beta > 0.5$  beyond 10 kpc. We also consider  $\beta$  as a function of time for individual simulated galaxies, discuss when and why “dips” in  $\beta$  form<sup>10</sup> and the rarity of  $\beta < 0$  values, and discuss the origin and persistence of these dips in the in situ and accreted halo. We also highlight one simulation that is a  $\beta(r)$  outlier: while this galaxy appears to be a normal MW-like disk galaxy at the present day, it

<sup>10</sup> Our fiducial definition of a “dip” is a value of  $\beta$  that is at least  $0.2$  lower than  $\beta$  at the surrounding radii.

experienced a major merger with a gas-rich system at  $z \sim 1$ . This event left a lasting imprint on the spherically averaged value of  $\beta(r)$ ; the stellar halo has a “trough”  $\beta$  profile—a persistently low positive to negative value of  $\beta$  over a wide range of radii—until the present day. We note that this isotropic to tangential  $\beta$  feature is not uniform across the sky; however, it is observable in at least a quarter to half of the sky at any given radius. We speculate that if the MW went through a similar cataclysmic event, then the signature in  $\beta(r)$  should be visibly present in the MW’s stellar halo today and measurable in the foreseeable future. If, on the other hand, the narrow dip at  $r \sim 20$  kpc is confirmed or other dips are found, we suggest that these are ideal locations to carry out a follow-up search for either substructure or in situ halo stars. These two possibilities can be distinguished by the metallicity and  $\alpha$ -abundance patterns of the stars giving rise to the  $\beta$  dip. We discuss these results and draw further conclusions in Section 4.

## 2. Simulations

We analyze three different suites of high-resolution MW-like stellar halo simulations: a hybrid  $N$ -body + semi-analytic suite and two fully  $N$ -body+SPH suites with differing prescriptions for star formation and stellar feedback.

### 2.1. Suite from Bullock & Johnston

We consider 11 stellar halos from Bullock & Johnston (2005, BJ05), which are modeled using the hybrid  $N$ -body + semi-analytic approach. These models are publicly available<sup>11</sup> and are described in detail in Bullock & Johnston (2005), Robertson et al. (2005), and Font et al. (2006).

BJ05 assumes a  $\Lambda$ CDM framework with a cosmology of  $\Omega_m = 0.3$ ,  $\Omega_\Lambda = 0.7$ ,  $\Omega_b h^2 = 0.024$ ,  $h = 0.7$ . The authors generate 11 merger histories for a dark matter halo with  $z = 0$ ,  $M_{\text{vir}} = 1.4 \times 10^{12} M_\odot$  using the method described in Somerville & Kolatt (1999). For each merger event above  $5 \times 10^6 M_\odot$ , an  $N$ -body simulation of a dark matter satellite disrupting in an analytic, time-dependent galaxy + spherical dark matter halo is modeled. The baryonic component of each satellite is modeled using semi-analytic prescriptions and the star formation is truncated soon after each satellite halo is accreted on the MW host.

While BJ05 neglect satellite–satellite interactions and lack a responsive “live” halo and central galaxy, their methods have provided robust predictions for the spatial and velocity structure of stellar halos and streams in the outer parts of galaxies ( $\geq 20$  kpc), as well as reasonable estimates for global stellar halo properties from accreted material (mass and time evolution) at all radii (Bell et al. 2008). Moreover, their models sample a wide range of merger histories within allowable bounds for the MW, which makes them valuable for gaining intuition about the effects of mergers on the phase-space distribution of the stellar halo at the present day.

### 2.2. g14 Suite

We use the g14 (Christensen et al. 2012) suite of simulations, which contains four cosmologically derived (Spergel et al. 2003, WMAP3) MW-mass galaxies named g14\_h239, g14\_h258, g14\_h277, and g14\_h285; these galaxies are evolved to redshift zero using the parallel  $N$ -body+SPH

code GASOLINE (Wadsley et al. 2004). These runs have a spatial resolution of 170 pc and mass resolutions of  $1.3 \times 10^5$ ,  $2.7 \times 10^4$ , and  $8.0 \times 10^3 M_\odot$  for the dark matter, gas, and stars, respectively, while also including the large-scale environment by using the “zoom-in” volume renormalization technique (Katz & White 1993) to create the initial conditions. The simulations use a redshift-dependent cosmic UV background and realistic cooling and heating, including cooling from metal lines (Shen et al. 2010). Supernovae feedback is modeled using the “blastwave” approach (Stinson et al. 2006), in which cooling is temporarily disabled based on the local gas characteristics. The probability of star formation is a function of the non-equilibrium  $H_2$  abundances (Christensen et al. 2012). The result of tying the star formation to the molecular hydrogen abundance is a greater concentration of the stellar feedback energy and the more efficient generation of outflows. These outflows ensure that the final galaxies have appropriate rotation curves (Governato et al. 2012), stellar mass fractions (Munshi et al. 2013), and dwarf satellite populations (Zolotov et al. 2012; Brooks & Zolotov 2014).

### 2.3. MaGICC Suite

We utilize two cosmological hydrodynamic simulations named MaGICC\_g1536 and MaGICC\_g15784, from the Making Galaxies in a Cosmological Context (MaGICC, Stinson et al. 2013) suite of simulations. Like the g14 suite, the MaGICC galaxies were generated using GASOLINE (Wadsley et al. 2004); however, instead of disabling cooling at early times, the MaGICC implementation includes early stellar feedback from massive stars, which is purely thermal and operates much like an ultraviolet ionization source. The early heating of the gas suppresses a higher fraction of star formation prior to  $z = 1$  than supernovae feedback alone; thus, the MaGICC galaxies do not suffer from overcooling, and have realistic rotation curves (see Figure 1 of Santos-Santos et al. 2016) with smaller central bulges in the MW host galaxies and more realistic stellar content in satellite galaxies.

The MaGICC simulations contain dark matter, gas, and star particles with masses of  $1.11 \times 10^6 M_\odot$ ,  $2.2 \times 10^5 M_\odot$ , and  $< 6.3 \times 10^4 M_\odot$ , respectively, and a gravitational softening length of 310 pc. The two MaGICC galaxies we analyze, MaGICC\_g1536 and MaGICC\_g15784, have previously been studied extensively (see Snaith et al. 2016 and references therein).

For both the MaGICC and g14 simulations, halo membership is determined using the density-based halo-finding algorithm AHF (Gill et al. 2004; Knollmann & Knebe 2009). We previously analyzed the in situ and accreted stellar halo from MaGICC\_g15784 in Valluri et al. (2016); in this work, any star belonging to the primary halo at the present day is classified as either an in situ star or an accreted star. Stars that are born in the primary halo are classified as in situ stars, while stars that are born in other bound structures are classified as accreted. Because we are interested in the kinematic properties of the stellar halo, we distinguish between in situ halo and in situ disk stars based purely on a spatial cut; at the present day, any in situ stars with  $|z| > 5$  kpc are considered to be in situ halo stars.<sup>12</sup> For MaGICC\_g1536, 24% of the halo stars

<sup>11</sup> Found at <http://www.astro.columbia.edu/~kvj/halos/>.

<sup>12</sup> Throughout this work, we orient each simulated MW-like galaxy with its angular momentum vector pointed along the  $z$ -axis, ensuring its disk is aligned in the  $x$ - $y$  plane.



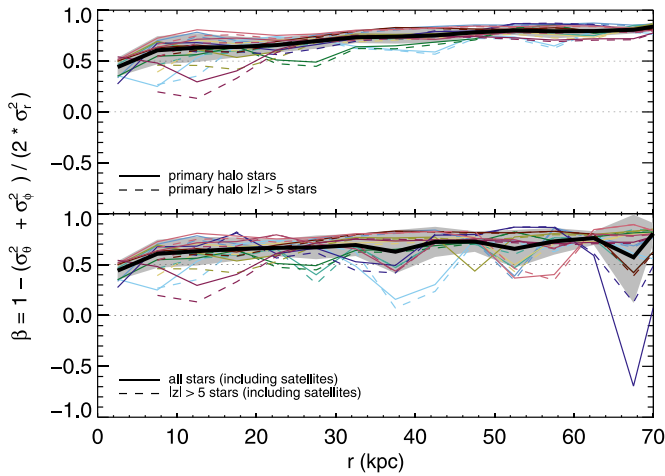


**Figure 1.**  $\beta$  as a function of radius for 11 stellar halos from BJ05. Top panel:  $\beta$  for stars belonging to the primary halo at the present day. Thin lines correspond to individual halos and the thick line corresponds to average behavior; shaded gray shows area within  $1\sigma$  of the mean. Solid lines correspond to all stars and dashed lines correspond to stars with  $|z| > 5$  kpc. Bottom panel:  $\beta$  for all stars within the virial radius (including satellites) at the present day. The thin, thick, solid, and dashed lines and shaded region are the same as in the top panel.

are in situ halo stars, and for the more massive system, MaGICC\_g15784, 42% of the halo stars are in situ halo stars.

### 3. Results

#### 3.1. Radially Anisotropic Trends

We begin by considering the  $z = 0$  behavior of  $\beta(r)$  for the BJ05 suite of simulations. As noted in Section 2.1, the BJ05 models are produced using a hybrid  $N$ -body + semi-analytic approach, which results in stellar halos formed purely from accreted material. Henceforth, we adopt a fiducial radial bin size of 5 kpc.

The top panel of Figure 1 presents  $\beta(r)$  for the BJ05 models for stars that belong to the primary halo at the present day. The behavior of each individual halo is shown by thin lines, while the average behavior of all 11 halos is shown by the thick black solid line surrounded by the  $1\sigma$  error bands shaded in gray. As a check, we look at  $\beta(r)$  for two cuts on the data: all the stars in the stellar halo (solid line), and just the stars with  $|z| > 5$  kpc (dashed line). There is no difference in the average  $\beta(r)$  values for these two populations. As also shown in Williams & Evans (2015), the average trend in the BJ05 suite is quite radially biased at all radii. From the smallest radial bin outward,  $\beta \geq 0.5$ ; by  $r \sim 30$  kpc,  $\beta \sim 0.7$ , and for larger  $r$ ,  $\beta$  asymptotes to  $\sim 0.8$ . Regardless of merger history, all 11 halos show the same global behavior, trending toward large values of  $\beta$  at large  $r$ . In fact, the halo with a large late-time accretion event (halo 9, shown in green) is relatively indistinguishable in  $\beta$  from the other 10 halos. While there are slight dips in  $\beta$  for individual halos, these dips never plummet to tangential or even isotropic values. Most dips are fairly small (of the order of 0.2–0.3 lower than the average  $\beta$  value), and beyond  $r \sim 20$  kpc, even these dips do not descend below  $\beta \sim 0.5$ .

The bottom panel of Figure 1 presents  $\beta(r)$  for all stars in the simulation, including those bound to infalling satellites. Because stars in a satellite lie within a small spatial volume and follow a coherent trajectory, including satellites generates dips in individual  $\beta(r)$  profiles; these dips are  $\sim 5$ –15 kpc wide. A significant number of these dips fall below  $\beta \sim 0.5$ ;

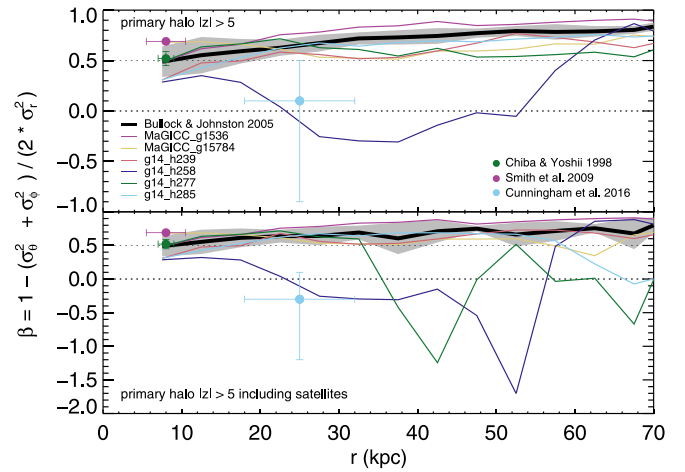


**Figure 2.** Top panel:  $\beta(r)$  profiles for all stars belonging to the primary stellar halos from six cosmological simulations (colored lines) and the average profile from BJ05 simulations (thick black curve), with the region within  $1\sigma$  of the mean for BJ05 shown in gray. Only one galaxy (g14\_h258) shows significant (negative) deviation from the average curve over a large range of radii (see Section 3.2.3 for details). The three points mark three measurements of  $\beta$  in the MW from 6D coordinates. Bottom panel: same as above for all stars including those bound to satellites within the virial radius at the present day.

however, unexpectedly, very few of the dips could be considered isotropic and only one is tangential. Moreover, in the tangential instance (dark blue curve), it is very clear that the stars generating the dip belong to a small, coherent structure; this can be seen from the substantial difference in  $\beta$  for the full sample and the  $|z| > 5$  kpc sample at  $r \sim 65$  kpc.

We consider next the individual trends in the six  $N$ -body +SPH simulations from the g14 and MaGICC suites. Here we select stars belonging to the stellar halo by a spatial cut ( $|z| > 5$  kpc). The top panel of Figure 2 shows  $\beta(r)$  for the stars that belong to the primary halo at the present day. Plotted in black is the average trend from Figure 1, with the  $1\sigma$  error band plotted in gray. Five of the six galaxies follow the BJ05 trend: from  $r \sim 10$ –15 kpc onward,  $\beta \geq 0.5$ . For these galaxies,  $\beta$  never falls below 0.5 and it generally trends toward larger values with increasing radius. While these five galaxies represent a wide range of merger histories for  $z < 1$ , their  $\beta(r)$  behaviors are remarkably consistent with one another: g14\_h239 (shown in salmon) has the most active merger history and yet its  $\beta(r)$  is virtually indistinguishable from that of g14\_h277 (shown in green), which has a remarkably quiescent merger history until the very end of the simulation. Interestingly, the one galaxy that does not follow the BJ05 trend, g14\_h258, has a somewhat unremarkable merger history for  $z < 1$ . We will discuss this galaxy further in Section 3.2.3. It is remarkable, though, that none of the simulations' minor mergers from  $z < 1$  leaves a lasting impression on  $\beta(r)$ .  $\beta$  is predicted by the average trends in BJ05, g14, and MaGICC suites to be  $\sim 0.5$  or larger at all radii beyond  $r \sim 8$  kpc at the present day.

The three individual data points on Figure 2 mark existing measurements based on 6D data in the MW from nearby stars falling within  $\sim 2$  kpc from the Sun (Chiba & Yoshii 1998), from SDSS stars in Stripe 82 within 5 kpc of the Sun (Smith et al. 2009), and from 13 HALO7D stars lying within  $18 < r/\text{kpc} < 32$  (Cunningham et al. 2016). Note that the measurements of anisotropy from nearby stars (green point) and SDSS (salmon point) are completely consistent with predictions from

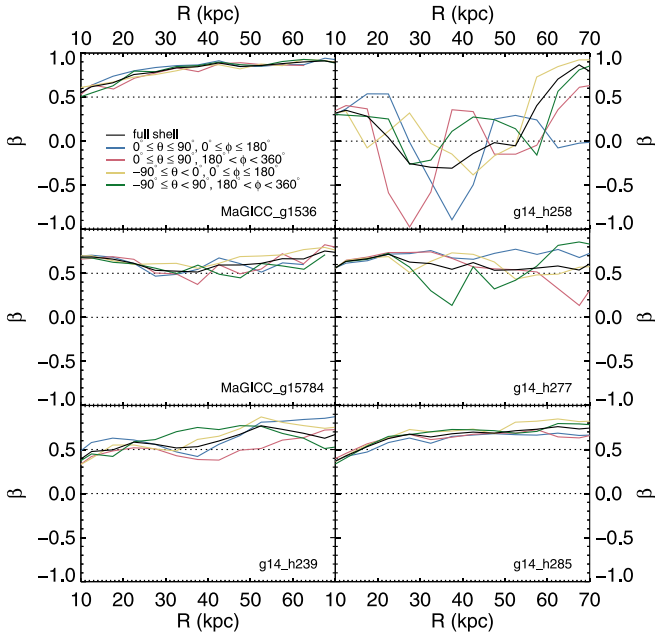


**Figure 3.**  $\beta(r)$  profiles by angular quadrants for the six cosmological hydrodynamic simulations considered in Figure 2. For each galaxy, the total  $\beta(r)$  profile is shown in black, and the  $\beta(r)$  profiles for the angular quadrants ( $0^\circ < \theta < 90^\circ$ ,  $0^\circ < \phi < 180^\circ$ ), ( $0^\circ < \theta < 90^\circ$ ,  $180^\circ < \phi < 360^\circ$ ), ( $-90^\circ < \theta < 0^\circ$ ,  $0^\circ < \phi < 180^\circ$ ), and ( $-90^\circ < \theta < 0^\circ$ ,  $180^\circ < \phi < 360^\circ$ ) are shown in blue, salmon, yellow, and green, respectively. With the exception of g14\_h258, the total behavior closely mimics the quadrant behavior except where a galaxy is actively accreting a satellite (as in the case of g14\_h277). Outlier g14\_h258 shows a complex angularly and radially dependent  $\beta(r)$  signature, which we discuss in further detail in Section 3.2.3.

all the simulations. The error bars on the measurement from HALO7D (pale blue point) are large but the measured value, while still positive in the top panel, is significantly lower than the predictions from most of the simulations and intriguingly is consistent with the predictions from g14\_h258.

The bottom panel of Figure 2 presents  $\beta(r)$  for all stars in the simulation inside the virial radius of the primary halo but with  $|z| > 5$  kpc, including those bound to infalling satellites. Here, it is obvious that three of the six galaxies are interacting with satellites at the present day: g14\_h277, g14\_h285, and MaGICC\_g15784. The first two of these galaxies have strongly tangential dips in  $\beta$ . These dips are much stronger than the tangential dip seen in BJ05. The dip in MaGICC\_g15784 ( $\beta \sim 0.4$ ) is still a radial value, but it would be stronger if the satellite were aligned differently with the disk, because it falls within  $|z| < 5$  kpc at the end of the simulation.

Building on this, we next explore how uniform  $\beta$  is across the sky. Figure 3 shows the  $\beta(r)$  profiles for the six hydrodynamic simulations from Figure 2, but now subdivided by angular quadrants. The four non-overlapping angular quadrants that we consider are ( $0^\circ < \theta < 90^\circ$ ,  $0^\circ < \phi < 180^\circ$ ), ( $0^\circ < \theta < 90^\circ$ ,  $180^\circ < \phi < 360^\circ$ ), ( $-90^\circ < \theta < 0^\circ$ ,  $0^\circ < \phi < 180^\circ$ ), and ( $-90^\circ < \theta < 0^\circ$ ,  $180^\circ < \phi < 360^\circ$ ). For each galaxy, the total  $\beta(r)$  profile from Figure 2 is shown in black, while the  $\beta(r)$  profile for each angular quadrant is shown by a colored line.

At a given radius is  $\beta$  the same in every direction we look? By and large, yes, it is the same in every direction we look for the five “typical” hydrodynamic simulations. The total behavior closely mimics the quadrant behavior except where a galaxy is actively accreting a satellite, as in the case of g14\_h277. However, the one outlier galaxy, g14\_h258, shows a

complex angularly and radially dependent  $\beta(r)$  signature. We discuss this galaxy in further detail in Section 3.2.3. Overall, we conclude that unless a galaxy is actively accreting a satellite or experienced a unique cataclysmic merger,  $\beta$  is self consistent across the sky at a given radius.

We conclude from this analysis of 17  $z = 0$  MW-like stellar halos that, except in the rarest of cases,  $\beta(r)$  is strongly predicted to be radially anisotropic beyond  $r \sim 8$  kpc. In fact, the average trends for all three suites of simulations predict that  $\beta \sim 0.5$  or larger at all radii at the present day.

### 3.2. Deviations from Radial Anisotropy

As we have shown, a robust prediction of  $\Lambda$ CDM simulations is that stellar halos are radially anisotropic ( $\beta \geq 0.5$ ). However, recent analysis of 6D MW data indicates a low value of  $\beta$  at larger radii in our galaxy (Cunningham et al. 2016); these observations prompt us to explore when and how rare departures from radial anisotropy occur in simulations. In what follows, we conduct a time series investigation of two hydrodynamic simulations, MaGICC\_g15784 and g14\_h258; we explore three different scenarios when deviations from radial anisotropy occur:

1. An ongoing accretion event can cause a short-lived ( $\Delta\text{time} < 0.2$  Gyr) dip in  $\beta$  over a small range in radii.
2. Close passage of a large satellite galaxy can cause a longer-lived ( $\Delta\text{time} \geq 0.4$  Gyr) dip in  $\beta$  in the in situ halo over a small range in radii.
3. A major merger event can cause a very long-lived ( $\Delta\text{time} \sim 7$  Gyr) tangential  $\beta$  feature across a large range of radii and a large angular fraction of the sky.

Here we illustrate each of these scenarios in turn.

#### 3.2.1. Transient $\beta$ Dips in the Total Stellar Halo

We now consider the total stellar halo for MaGICC\_g15784, which is dominated by accreted stars beyond  $r \sim 30$  kpc and is slightly oblate with a short/long axis ratio  $c/a \sim 0.85$ . At  $z = 0$ , MaGICC\_g15784 has a virial radius  $R_{200} = 214$  kpc, a virial mass  $M_{200} = 1.2 \times 10^{12} M_\odot$ , and a stellar mass  $M_* = 8.3 \times 10^{10} M_\odot$ <sup>13</sup>, and it experienced its last major merger at  $z \sim 1$ .

The left panel of Figure 4 illustrates the spatial distribution (in Galactocentric cylindrical coordinates,  $z$  versus  $R$ ) of stars in the stellar halo at time  $\sim 10.5$  Gyr (redshift  $z \sim 0.3$ ). The gray shaded region corresponds to a spherical shell spanning  $40 < r/\text{kpc} < 60$  and containing a stellar halo mass of  $7.2 \times 10^7 M_\odot$ , which we look at in detail in the other three panels of Figure 4. At 10.1 Gyr, a bound satellite (stars shown in blue) enters the gray shaded region; this satellite contains a total stellar mass of  $2.6 \times 10^6 M_\odot$ . The black arrows show the direction of movement of the satellite. As it moves up through the mid-plane, it is disrupted and no longer identified by the halo-finding algorithm as a unique object. However, stars from this satellite maintain coherence for several time steps, as illustrated by the location of these stars at 10.3 and 10.5 Gyr (shown in red and dark green in the left panel of Figure 4).

The top right panel of Figure 4 shows  $\beta(r)$  for 10.1, 10.3, and 10.5 Gyr for stars falling within  $40 < r/\text{kpc} < 60$  and

<sup>13</sup> Here we have defined the virial radius to be  $R_{200}$ , the radius at which the average density of the halo is 200 times the critical density of the universe, and the virial mass to be the total mass within the virial radius.

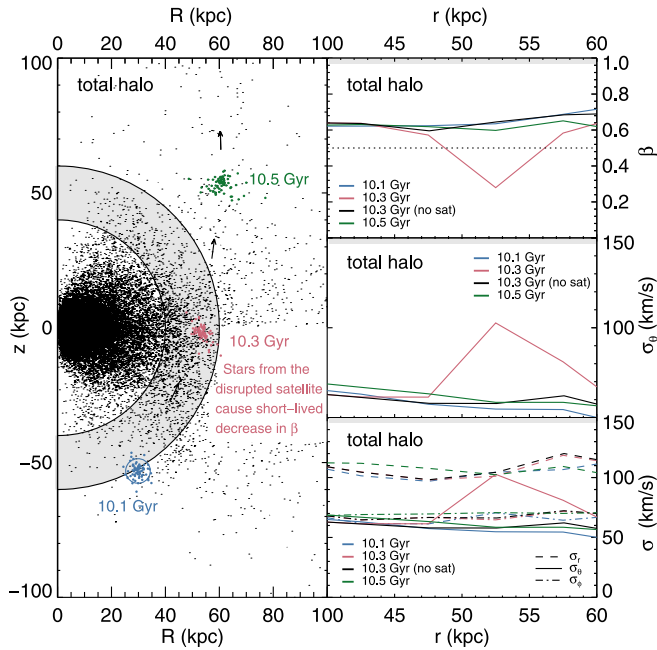


**Figure 4.** Illustration of the formation of a short-lived “dip” in  $\beta$  in the total (accreted + in situ) stellar halo of MaGICC\_g15784. Left: the black points show the total stellar halo (in cylindrical coordinates) at 10.5 Gyr. The gray shaded region between the solid curves marks the radial shell for which  $\beta$  and  $\sigma$  profiles are shown in the other panels. Colored points mark the location of stars belonging to a disrupting satellite as it passes through the MW-like galaxy MaGICC\_g15784 at three different times (blue, red, and dark green corresponding to times  $\sim 10.1$ , 10.3, and 10.5 Gyr); the circle on top of the stars at 10.1 Gyr indicates that the satellite is bound at this time. All of these stars are identified as belonging to MaGICC\_g15784’s stellar halo by time  $\sim 10.3$  Gyr. The black arrows mark the trajectory of the stars as the satellite breaks up. Top right:  $\beta(r)$  profiles for the total stellar halo at three different times (with and without the stars from the disrupted satellite at  $t = 10.3$  Gyr). Middle right: the corresponding polar velocity dispersion. Bottom right: all three components of the velocity dispersion for the total halo stars.

belonging to the total stellar halo at those time steps. At 10.1 Gyr, the bound satellite enters the shell at  $40 < r/\text{kpc} < 60$ . The  $\beta$  anisotropy at 10.1 Gyr is greater than 0.6 at all radii within the volume; at this time, the stars that belong to the satellite are not considered a part of the stellar halo, and thus  $\beta(r)$  is not impacted by it. However, by 10.3 Gyr, the satellite has fully disrupted and stars from it are now considered a part of the total stellar halo; at this time a strong dip to  $\beta \sim 0.25$  appears at  $50 < r/\text{kpc} < 55$  (shown in red). This dip arises because stars from the disrupted satellite, which now lie inside this radial range, are on a polar orbit (as seen in the left panel) and hence their net orbital motion adds to the dispersion in the  $\theta$  direction. The former satellite’s contribution can be seen clearly by contrasting  $\beta(r)$  for all the stars in the stellar halo (red line) to  $\beta(r)$  excluding the former satellite’s stars (black line). The black line is greater than  $\sim 0.6$  at all radii, just like  $\beta(r)$  at 10.1 Gyr. At 10.5 Gyr,  $\beta(r)$  is no longer impacted by the former satellite in the range of radii under consideration, because the stars from the former satellite have moved out of the spherical shell.

Why does a dip form with the addition of the recently stripped stars? The middle right panel of Figure 4 shows  $\sigma_\theta$  at 10.1 (blue line), 10.3 (salmon line), and 10.5 (green line) Gyr. Clearly,  $\sigma_\theta$  is substantially enhanced by adding the satellite stars; however,  $\sigma_\phi$ ,  $\sigma_r$  remain unchanged (see bottom right panel of Figure 4). This is because (as can be seen in the left

panel) the satellite is on a predominantly polar orbit and hence the satellite debris has a large  $v_\theta$ . Again, when we remove stars from the disrupted satellite at 10.3 Gyr (black line) the dip in  $\sigma_\theta$  disappears, confirming that this coherent substructure is the source of the dip in  $\beta$ . Note, in this instance, that an inspection of the stellar halo’s  $v_\theta$  distribution indicates the presence of the satellite debris with a slight overdensity of stars at larger values of  $v_\theta$ . However, even in this case, we emphasize that  $\beta(r)$  is an instructive complementary tool, which allowed us to quickly home in on an interesting radial bin with minimal effort.

We track the disrupted satellite for several more time steps and find that the  $\beta$  dip does occur at larger radii, albeit to a lesser extent. This is because, as the disrupted satellite continues on its original orbit, it becomes increasingly radial. We note that this does not explain why the recently accreted stars do eventually turn radially anisotropic; however, the particulars of that transition are outside the scope of this paper to explore.

We conclude that dips in  $\beta$  generated in the total stellar halo are short-lived (lifetime  $< 0.2$  Gyr) and closely tied to recent accretion events. We suggest that hunting for such dips in velocity anisotropy, particularly at large radii, may be an effective means for identifying recently accreted but somewhat dispersed material.

### 3.2.2. $\beta$ Dips in the in situ Stellar Halo

We now consider MaGICC\_g15784’s in situ stellar halo within  $25 < r/\text{kpc} < 45$  between 11.8 and 12.9 Gyr. As noted in Section 2.3, in situ halo stars are distinguished from in situ disk stars by a spatial cut at  $z = 0$ . At 11.8 Gyr, the numbers of in situ and accreted halo stars are roughly equal at 25 kpc, although the in situ stars are more concentrated toward the plane of the disk. Their kinematic behavior is also different; we see evidence of this in the response of the in situ stellar halo to the passage of a large, gas-rich satellite ( $M_{\text{total}} = 4.4 \times 10^{10} M_\odot$ , roughly twice the mass of the Small Magellanic Cloud; Besla et al. 2012) through the volume at 12.3 Gyr.

The left panel of Figure 5 illustrates the spatial distribution (in Galactocentric cylindrical coordinates,  $z$  versus  $R$ ) of stars in the in situ stellar halo at time  $\sim 12.3$  Gyr. The gray shaded region corresponds to a spherical shell spanning  $25 < r/\text{kpc} < 45$ , which we look at in detail in the other five panels of Figure 5. The unfilled circles show the location of the large satellite that passes through the volume at 11.8, 12.1, 12.3, 12.7, and 12.9 Gyr with black arrows indicating the direction of motion over time. At 12.3 Gyr, the satellite begins its passage through the region in question, but by 12.7 Gyr, it has moved beyond the relevant volume. Note that no stars are donated by the satellite to the stellar halo during this passage, nor would such an exchange impact the in situ stellar halo, because in situ stars are by definition produced only in the primary halo.

The top right panel of Figure 5 shows  $\beta$  for all five moments in time for the in situ stars from the gray shaded region. Note that we require at least 20 star particles within each radial bin to calculate  $\beta$ , and within  $30 < r/\text{kpc} < 35$  there are at least 125 in situ halo star particles at each time step. Before the satellite interacts with MaGICC\_g15784,  $\beta$  for the in situ stellar halo is consistent with the average behavior of BJ05; as can be seen by the dark and light blue lines for  $\beta$  at 11.8 and 12.1 Gyr respectively,  $\beta$  is either  $\sim 0.5$  or larger at all radii in question and is as high at  $\sim 0.7$  in the range  $30 < r/\text{kpc} < 35$  at 12.1 Gyr. However, starting from 12.3 Gyr onward,  $\beta$  dips



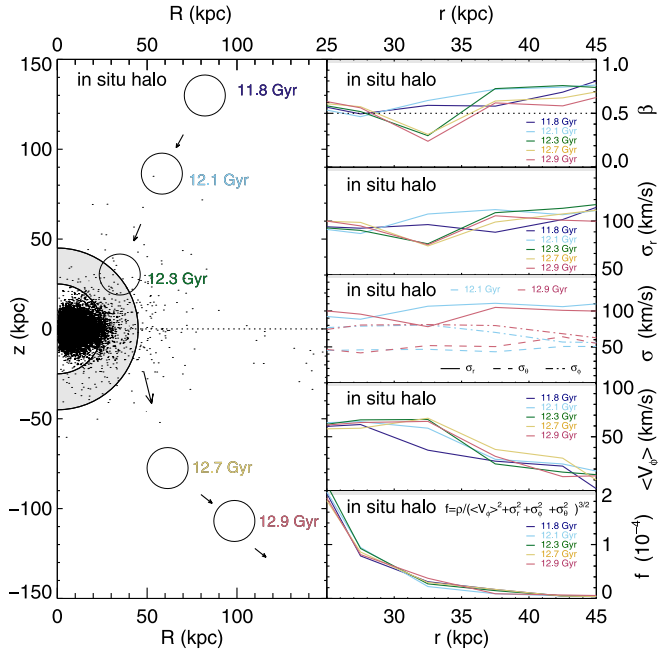


**Figure 5.** Illustration of the formation of a long-lived “dip” in  $\beta$  in the in situ stellar halo of MaGICC\_g15784. Left: the black points show the in situ stellar halo (in cylindrical coordinates) at 12.3 Gyr. The gray shaded region between solid curves marks the radial shell for which  $\beta$  and  $\sigma$  profiles are shown in other panels. The open circles correspond to the position of a large satellite with  $M_{\text{total}} = 4.4 \times 10^{10} M_{\odot}$  (roughly twice the mass of the Small Magellanic Cloud; Besla et al. 2012) at five different times as indicated by the labels; black arrows mark the trajectory of the satellite. Top right:  $\beta(r)$  profiles for the in situ stellar halo at the five different times. Second from the top right: the corresponding radial velocity dispersion. Middle right: all three components of velocity dispersion for the in situ halo stars before and after the satellite interaction. Second from the bottom right: the corresponding mean azimuthal velocity profile at all five times. Bottom right: the (pseudo) coarse-grained phase-space density quantity,  $f = \rho / (\langle v_{\phi} \rangle^2 + \sigma_r^2 + \sigma_{\phi}^2 + \sigma_{\theta}^2)^{3/2}$  in units of  $10^{-4}$ . Note that  $f$  is  $\sim$ constant with time, suggesting that this proxy for phase-space density is conserved.

sharply to 0.2–0.3 in the range  $30 < r/\text{kpc} < 35$ . This dip persists until the present day. Other such long-lasting in situ  $\beta$  dips are found elsewhere in MaGICC\_g15784 and MaGICC\_g1536 and are coincident with the passage of a  $\sim 1.0 \times 10^{10} M_{\odot}$  satellite through the plane  $z = 0$ ; however, in all these other cases, the in situ  $\beta$  dips are radially anisotropic ( $\beta > 0$ ).

The kinematically hotter accreted stellar halo does not experience a similar dip in  $\beta$  at this radius at this epoch. So why does the in situ  $\beta$  dip form and persist in this case? As can be seen in the second from the top panel on the right of Figure 5,  $\beta$  declined within  $30 < r/\text{kpc} < 35$  because  $\sigma_r$  decreases at 12.3 Gyr. However, as can be seen in the middle right panel of Figure 5, neither  $\sigma_{\phi}$  nor  $\sigma_{\theta}$  is appreciably altered. At the same time, it is clear that there is an increase in the mean streaming motion in this volume  $\langle v_{\phi} \rangle$  (see the second from the bottom right panel of Figure 5). This increase appears to result from torquing on the in situ halo stars originating from the passage of the massive satellite, which imparts angular momentum to them. During the encounter the satellite (which is moving retrograde relative to the rotation of g15784’s disk) loses orbital angular momentum. The increase in angular momentum of the in situ halo stars results in a corresponding decrease in  $\sigma_r$ . Note that we have computed the pseudo phase-space density,  $\rho / (\langle v_{\phi} \rangle^2 + \sigma_r^2 + \sigma_{\phi}^2 + \sigma_{\theta}^2)^{3/2}$ , for the in situ halo stars

(bottom right panel of Figure 5), and it is clear that the radial profile of this quantity does not change during the interaction. This constancy in the coarse-grained phase-space density profile is reminiscent of the Liouville theorem although we caution that  $f$  is not the fine-grained phase-space density, to which the Liouville theorem applies. This suggests that the reason that the dip in  $\beta$  persists in this case is that the stars contributing to the dip have had their kinematic and density distributions permanently altered in a way that results in a long-term equilibrium.

As noted in earlier studies, the in situ stellar halo is on average more metal-rich and has a lower  $\alpha$ -abundance than the accreted stellar halo (Zolotov et al. 2009; Tissera et al. 2013; Pillepich et al. 2015). In Valluri et al. (2016) and S. R. Loebman et al. (2017, in preparation), we analyze the ages, metallicity, and orbits of accreted and in situ stellar halos in the MaGICC suite, and we also find that the in situ halo stars are on average more metal-rich (on average 0.7 dex higher metallicity) and have a lower  $\alpha$ -abundance than the accreted halo stars in the same volume. While our detailed analysis of the connection between metallicity and in situ origin is forthcoming, we speculate that if  $\beta$  dips are identified in observational data sets, then metallicity could be used to help distinguish their origin. Did these halo stars form in a small satellite that was recently disrupted? This accretion origin would correspond to a low to average metallicity in the stellar halo at this radius. Or did they form in the MW? This in situ origin would correspond to a higher metallicity than in stars at neighboring radii in the stellar halo.

### 3.2.3. Merger-induced $\beta$ Trough

We consider now the  $\beta(r)$  outlier, g14\_h258, shown in dark blue in Figure 2 and the top right panel in Figure 3. Like the other galaxies in the g14 suite, g14\_h258 is a good proxy for the MW at  $z = 0$  by total mass, total stellar mass, and bulge-to-disk ratio (Governato et al. 2009; Christensen et al. 2012); however, as discussed in Governato et al. (2009), g14\_h258 experiences a major merger (mass ratio of merging halos 1.2:1) at  $z \sim 1$ . At this time, the progenitor galaxies plunge in on fairly radial orbits, with the internal spins of the two disks roughly aligned with the orbital angular momentum vector (see Figure 1(a) of Governato et al. 2009). Over 1 Gyr, the progenitors experience two close passages, and they finally coalesce at  $z \sim 0.8$ , thickening the stellar disks and populating the stellar halo in the process. From  $z \sim 0.8$  onward, the system has a relatively quiescent merger history as it regrows its thin disk through accreted gas.

In the top left panel of Figure 6, we consider  $\beta(r)$  over time for g14\_h258. Before the major merger occurs at  $z \sim 1.2$  (shown in salmon),  $\beta(r)$  is consistent with the average profile for BJ05 for  $r < 30$  kpc. While  $\beta(r)$  does show a dip at  $r \sim 45$  kpc due to a satellite interaction, this dip is minor (neither isotropic nor tangential).

However, for every time step for  $z < 1$ ,  $\beta(r)$  shows a tangential to isotropic profile over a wide range of radii. That is, the imprint of the  $z \sim 1$  merger event is encoded in the orbits of the halo stars. This can be seen clearly in the trends for each component of the velocity dispersion as a function of radius. The average trends for the five “normal” N-body+SPH galaxies from Figure 2 are shown in the top right panel of Figure 6; here  $\sigma_r > \sigma_{\phi} > \sigma_{\theta}$  at all radii. However, in the middle two panels and bottom left panel of Figure 6,



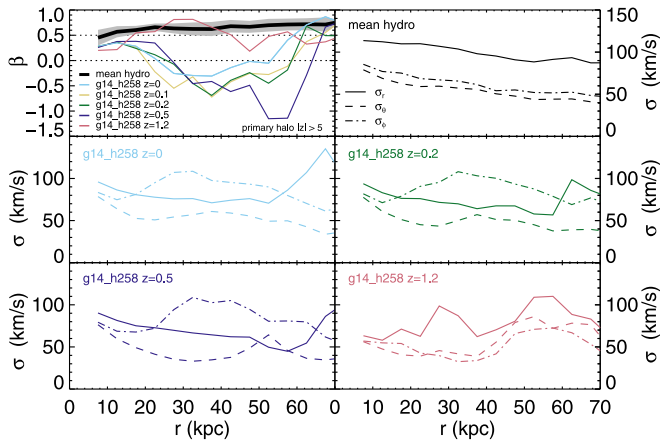


**Figure 6.** Signatures of major merger in g14\_h258. Top left:  $\beta(r)$  profiles at five different time steps compared with the mean  $\beta(r)$  for the halo stars from the other five hydrodynamic simulations. The remaining panels show radial profiles of  $\sigma_r$ ,  $\sigma_\theta$ , and  $\sigma_\phi$  for the mean of the five hydrodynamic simulations (top right) and for the four other time steps. The middle panels and bottom left panel correspond to times after the merger event and the bottom right panel corresponds to a time before the merger event.

$\sigma_\phi > \sigma_r > \sigma_\theta$  over the radii for which  $\beta(r) \leq 0$ . This is due to a significant enhancement in  $\sigma_\phi$  and a minor cooling/suppression in growth of  $\sigma_r$ .

Physically, why does this happen? A detailed analysis of velocity dispersion profiles and  $\beta$ -profiles in four different quadrants of the galaxy g14\_h258 at  $z = 0$  reveals that the trough in  $\beta$  results from multiple substantially narrower dips in  $\beta$ , each only about 10–30 kpc wide. Furthermore, each quadrant exhibits two distinct dips (see the top right panel of Figure 3 for a visualization of this). The trough in the global  $\beta$  profile arises because the dips in each quadrant occur at different radii and have different depths.

Interestingly, when we look at the stars that belonged to the satellite galaxy that merged with the system at  $z \sim 1$ , these stars are evenly dispersed at all radii and angular cross sections. However, when we look at the distribution of stars today that belonged to the progenitor of g14\_h258 at  $z \sim 1.4$ , we see an overdensity of stars that looks like a tidal tail that wraps nearly around the galaxy. When we look at  $\beta$  in different angular quadrants, we pick out regions that cross this tidal structure. That is, the  $\beta$  dip is, in fact, picking up stars that once belonged to the primary in situ disk but have been displaced in an extended tidal feature that enhances  $\sigma_\phi$ . While visually this extended tidal feature is hard to disentangle from the overall stellar halo today, it has persisted from  $z \sim 0.8$  until the present, and the merger has left a lasting fingerprint on its kinematics.

While a merger event such as the one seen in g14\_h258 may rarely occur, the kinematic record should be long-lasting, with  $\beta \leq 0$  over a wide range of radii at the present day. Hunting for a broad  $\beta$  trough in the global  $\beta$  profile of the MW could be of great value because it would give us deep insight into the MW’s major merger history. With the upcoming all-sky *Gaia* survey and several follow-up surveys to obtain line-of-sight velocities it will soon be possible to search for  $\beta$  dips in many different parts of the sky and to use these observations to construct a global  $\beta$  profile for the Galaxy.

#### 4. Discussion and Conclusions

The results and implications of this study are as follows.

1. Both accretion-only simulations and  $N$ -body+SPH simulations predict strongly radially anisotropic velocity dispersions in the stellar halos for most MW-like disk galaxies. The most robust observations in the MW at  $r = 5\text{--}10$  kpc give  $\beta = 0.5\text{--}0.7$ , which is consistent with predictions from simulations.
2. There are three situations in which low positive to negative values of  $\beta$  arise in these MW-like simulations:
  - (a) Transient passage and disruption of a satellite, which contributes a coherently moving group of stars to the stellar halo: such dips are short-lived and last no longer than  $\sim 0.2$  Gyr.
  - (b) Passage of a massive satellite (that stays bound) through the inner part of the stellar halo induces transient changes in the kinematics of in situ halo stars. Dips in the in situ halo are longer-lived (lasting  $> 0.2$  Gyr) and more metal-rich (on average  $\sim 0.7$  dex higher) than dips in the accreted halo.
  - (c) A major merger with another disk at high redshift ( $z \sim 1$ ) can generate a stellar halo with a  $\beta$  trough—which persists to the present day. Such a trough is likely to comprise multiple 10–30 kpc  $\beta$  dips occurring at a range of radii that collectively appear as an extended trough. These dips should be visible over a significant portion (at least one quarter to half) of the sky at any given radius.

Previous results for  $\beta$  at  $r \sim 20\text{--}30$  kpc in the MW based on proper motions (measured by the *Hubble Space Telescope* in the direction of M31) suggest that  $\beta$  could be nearly zero or even slightly negative (Deason et al. 2013b; Cunningham et al. 2016). Such a low value of  $\beta$  could arise from substructure (as has been proposed by Deason et al. 2013b). If upcoming *Gaia* data confirm this dip in  $\beta$ , we predict that, if it was produced by a recently disrupted satellite, the  $\beta$  dip should be fairly localized in radius and unlikely to extend to over a larger portion of the sky. If this dip is found to be present primarily in stars of higher metallicity than those typically found in the accreted stellar halo, it could point to the presence of an in situ stellar halo that was perturbed by the passage of a massive satellite. In the unlikely event that the dip is found over a large portion of the sky and is highly negative over a wide range of radii, it could point to a major merger with a disk in the past. Such a trough is likely to comprise multiple 10–30 kpc dips occurring at a range of radii. These broad dips should be seen over a large portion of the sky, and the severity of a given dip is likely to differ in different parts of the sky.

It is clear that dips in  $\beta$  in the MW are a sensitive probe of recent interactions with satellites and long ago interactions with other disk galaxies. Determining proper motions with *Gaia* and fully characterizing 6D phase space with future surveys like the *Wide Field Infrared Survey Telescope* (WFIRST, Spergel et al. 2015) will enable us to explore substructure in the stellar halo in a new way. We posit that  $\beta$  should be thought of as a tool for discovery, because it will enable us to find and follow-up on the building blocks of our stellar halo.

Finally, as mentioned in the introduction, one of the original motivations for determining the anisotropy parameter  $\beta$  is that this quantity appears in the spherical form of the Jeans equations (Jeans 1915), and knowledge of  $\beta(r)$  in the stellar halo would enable a determination of the mass profile of the MW’s dark matter halo. However, the assumption underlying

the use of the spherical Jeans equation is that the tracer population and the potential that it traces are relaxed (virialized) and in dynamical equilibrium. As we have seen, non-monotonic  $\beta$  profiles generally arise from substructure or perturbations, which are clear evidence for a halo out of dynamical equilibrium. Since unvirialized systems tend to have higher kinetic energy than virialized systems the assumption of virial equilibrium would lead to an overestimate in the halo mass. Furthermore, for a given 3D velocity dispersion, an inferred tangential anisotropy also results in a higher estimate of the dynamical mass. This implies that if  $\beta$  in the MW stellar halo is found to be negative due to its non-equilibrium state, then dynamical measurements of the halo mass that use  $\beta$  are likely to overestimate the mass of the dark matter halo.

We thank the anonymous referee for useful feedback; the final manuscript is much stronger for their questions and comments. S.R.L. also thanks Jillian Bellovary for the suggestion and support in exploring g14\_h258. S.R.L. acknowledges support from the Michigan Society of Fellows. S.R.L. was also supported by NASA through Hubble Fellowship grant HST-HF2-51395.001-A from the Space Telescope Science Institute, which is operated by the Association of Universities for Research in Astronomy, Incorporated, under NASA contract NAS5-26555. M.V. and K.H. are supported by NASA ATP award NNX15AK79G. V.P.D. is supported by STFC Consolidated grant ST/M000877/1. V.P.D. acknowledges being a part of the network supported by the COST Action TD1403 Big Data Era in Sky and Earth Observation. V.P.D. acknowledges the support of the Pauli Center for Theoretical Studies, which is supported by the Swiss National Science Foundation (SNF), the University of Zürich, and ETH Zürich, and George Lake for arranging for his sabbatical visit, during which time this paper was completed. V.P.D. acknowledges the Michigan Institute of Research in Astrophysics (MIRA), which funded his collaboration visit to the University of Michigan, during which research for this paper was completed.

## Appendix

### Prospects for Measuring a Dip in $\beta$ with *Gaia* Data

In this appendix we estimate how accurately  $\beta$  can be determined with *Gaia* data, under a few simple assumptions, by analyzing mock catalogs of K giants and blue horizontal branch (BHB) stars with realistic observational errors. We assume that the observational error on the line-of-sight velocity is small; this assumption is based on knowledge of current and future ground-based follow-up surveys, such as the *Gaia*-ESO survey (Gilmore et al. 2012). *Gaia*-ESO has attained line-of-sight velocity errors of the order of a few  $\text{km s}^{-1}$ ; these errors are approximately valid for tracer populations such as BHB stars (Xue et al. 2011) and K giants (Xue et al. 2014).

We generate our mock catalogs assuming that the density profile of the stellar halo is given by  $\rho(r) \propto r^{-3}$ . We assume that halo stars obey an anisotropic Gaussian velocity distribution specified by the velocity dispersions ( $\sigma_r$ ,  $\sigma_\phi$ ,  $\sigma_\theta$ ), and that the system has no net rotation. We also assume that these properties are independent of stellar type. In addition, we assume that the radial velocity dispersion is independent of  $r$  and is equal to  $\sigma_r = 220 \text{ km s}^{-1}/\sqrt{2} = 156 \text{ km s}^{-1}$ . We adopt two models for the tangential components of the velocity

**Table 1**  
Assumed Properties of Mock Stars

| Sample                 | K Giants             | BHB Stars            |
|------------------------|----------------------|----------------------|
| $(V - I)^a$            | 0.99 mag             | 0.5 mag              |
| $M_V^b$                | 1.53 mag             | 0.71 mag             |
| $\sigma_{\text{DM}}^c$ | 0.35 mag             | 0.10 mag             |
| $\sigma_v^d$           | 5 $\text{km s}^{-1}$ | 5 $\text{km s}^{-1}$ |

**Notes.**

<sup>a</sup>  $(V - I)$  color.

<sup>b</sup> Absolute  $V$  magnitude.

<sup>c</sup> Error in distance modulus.

<sup>d</sup> Error in line-of-sight velocity.

dispersion:

$$\frac{\sigma_\phi^2(r)}{\sigma_r^2} = \frac{\sigma_\theta^2(r)}{\sigma_r^2} = \begin{cases} E(r, 22.5 \text{ kpc}, 2.5 \text{ kpc}), & \text{(Model 1),} \\ E(r, 22.5 \text{ kpc}, 5 \text{ kpc}), & \text{(Model 2),} \end{cases} \quad (2)$$

where we define

$$E(r, c, w) = \begin{cases} \frac{3}{4} + \frac{1}{4} \cos\left[\frac{2\pi}{2w}(r - c)\right], & (c - w < r < c + w), \\ \frac{1}{2}, & \text{(otherwise).} \end{cases} \quad (3)$$

Both Models 1 and 2 have a constant value of  $\beta = 0.5$  at  $r < c - w$  and  $c + w < r$ , but  $\beta(r)$  dips in between, attaining its minimum value of  $\beta = 0$  at  $r = c = 22.5 \text{ kpc}$ . The parameter  $w$  determines the width of the low- $\beta$  region (dip), and the dip in Model 1 is sharp ( $w = 2.5 \text{ kpc}$ ) while in Model 2 it is broad ( $w = 5 \text{ kpc}$ ).

For each model, we generate 2000 stars that satisfy  $15 \text{ kpc} < r_{\text{obs}} < 30 \text{ kpc}$ ,  $|z_{\text{obs}}| < 5 \text{ kpc}$ , and  $|b| > 30^\circ$ . Here,  $r_{\text{obs}}$ ,  $|z_{\text{obs}}|$ , and  $b$  are the observed Galactocentric radius, vertical distance from the Galactic plane, and the Galactic latitude, respectively. The assumed distance modulus errors ( $\sigma_{\text{DM}}$ ) for K giants and BHB stars are shown in Table 1. The line-of-sight velocity error is always assumed to be  $\sigma_v = 5 \text{ km s}^{-1}$ . The assumed values of  $(V - I, M_V)$  for K giants and BHB stars are shown in Table 1, and these values are used to evaluate the end-of-mission *Gaia* proper-motion errors (with the publicly available code PyGaia<sup>14</sup>).

We generate two mock catalogs (Models 1 and 2) for each type of star (K giants and BHB stars). For each of these four mock catalogs, we performed Bayesian analysis (similar to that presented in Hattori et al. 2017 and Deason et al. 2017) to derive the posterior distribution of  $(\sigma_r, \sigma_\phi, \sigma_\theta)$ . Figure 7 shows the recovered  $\beta(r)$  profiles for each of our mock catalogs.

The top two panels of this figure show that, for the mock K giant samples, neither the broad nor the narrow dip in the  $\beta(r)$  profile can be recovered. This is mainly because the distance error for K giants (16%) is too large. For example, if the heliocentric distance of a K giant is 22.5 kpc, the associated distance error is 3.6 kpc, which is comparable to or larger than the radial extent of the dip,  $w$ , in our models. Thus, the sample stars with  $r_{\text{obs}} \simeq 22.5 \text{ kpc}$  are highly contaminated by foreground and background stars, so that the  $\beta$  dip is blurred.

<sup>14</sup> <https://github.com/agabrown/PyGaia>

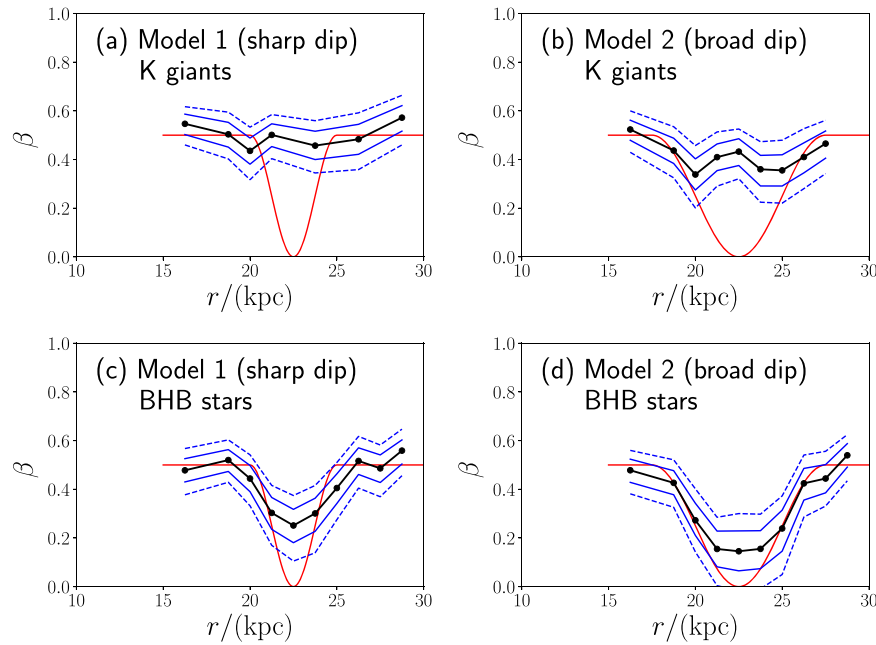


**Figure 7.** Mock analyses of K giant and BHB star catalogs with *Gaia*-like proper-motion error. The input profile of  $\beta(r)$  is shown by the red curve. The black dot shows the posterior median value of  $\beta$  at each radial bin. Blue solid and dashed lines covers 68% and 95% of the posterior distribution of  $\beta$ , respectively. We see that BHB stars are expected to be helpful in detecting dips in  $\beta$  due to their small distance uncertainty (5%), while K giants (distance error of 16%) are not.

When the mock BHB samples are used, the dips in the  $\beta(r)$  profiles are recovered easily, although the depths are underestimated. The dips in the BHB samples are more detectable than the dips in the K giant samples because the distance error for BHB stars (5%) is small. In Model 2, the recovered  $\beta$  profile is a very good match to the true  $\beta$  profile at  $15 \text{ kpc} < r < 30 \text{ kpc}$ . For both models, the depth of the recovered profiles is underestimated, but the location of the dips near  $r = 22.5 \text{ kpc}$  is recovered quite accurately.

These results suggest that in order to have the highest probability of detecting dips in the  $\beta(r)$  profile with *Gaia* proper-motion data, we need to use halo tracers whose distance error is smaller than the radial extent of the dip. Since the width (radial extent) of a dip is unknown a priori, it is desirable to use a population for which the distance errors are small, such as BHB stars. Although BHB stars are less numerous than K giants, more than 2000 stars within 30 kpc have already been observed (Xue et al. 2011). Since these BHB stars are brighter than the limiting magnitude of *Gaia*, proper motion will be obtained for all of them. It is therefore likely that *Gaia* data for BHB stars are capable of confirming the alleged dip in the  $\beta(r)$  profile at  $r \simeq 20 \text{ kpc}$  (e.g., Kafle et al. 2012; King et al. 2015).

### ORCID iDs

Sarah R. Loebman <https://orcid.org/0000-0003-3217-5967>  
 Monica Valluri <https://orcid.org/0000-0002-6257-2341>  
 Kohei Hattori <https://orcid.org/0000-0001-6924-8862>  
 Victor P. Debattista <https://orcid.org/0000-0001-7902-0116>  
 Eric F. Bell <https://orcid.org/0000-0002-5564-9873>  
 Charlotte R. Christensen <https://orcid.org/0000-0001-6779-3429>  
 Alyson Brooks <https://orcid.org/0000-0002-0372-3736>

### References

Abadi, M. G., Navarro, J. F., & Steinmetz, M. 2006, *MNRAS*, 365, 747  
 Bell, E. F., Zucker, D. B., Belokurov, V., et al. 2008, *ApJ*, 680, 295

Besla, G., Kallivayalil, N., Hernquist, L., et al. 2012, *MNRAS*, 421, 2109  
 Binney, J. 1980, *MNRAS*, 190, 873  
 Binney, J., & Tremaine, S. 2008, *Galactic Dynamics* (2nd ed.; Princeton, NJ: Princeton Univ. Press)  
 Bird, S. A., & Flynn, C. 2015, *MNRAS*, 452, 2675  
 Bond, N. A., Ivezić, Z., Sesar, B., et al. 2010, *ApJ*, 716, 1  
 Brooks, A. M., & Zolotov, A. 2014, *ApJ*, 786, 87  
 Bullock, J. S., & Johnston, K. V. 2005, *ApJ*, 635, 931  
 Chiba, M., & Yoshii, Y. 1998, *AJ*, 115, 168  
 Christensen, C., Quinn, T., Governato, F., et al. 2012, *MNRAS*, 425, 3058  
 Cunningham, E. C., Deason, A., Guhathakurta, P., et al. 2015, *IAUGA*, 22, 2255864  
 Cunningham, E. C., Deason, A., Guhathakurta, P., et al. 2016, *ApJ*, 820, 18  
 Deason, A. J., Belokurov, V., Evans, N. W., & An, J. 2012, *MNRAS*, 424, L44  
 Deason, A. J., Belokurov, V., Evans, N. W., & Johnston, K. V. 2013a, *ApJ*, 763, 113  
 Deason, A. J., Belokurov, V., Koposov, S. E., et al. 2017, *MNRAS*, 470, 1259  
 Deason, A. J., Van der Marel, R. P., Guhathakurta, P., Sohn, S. T., & Brown, T. M. 2013b, *ApJ*, 766, 24  
 Debattista, V. P., Moore, B., Quinn, T., et al. 2008, *ApJ*, 681, 1076  
 DESI Collaboration, Aghamousa, A., Aguilar, J., et al. 2016, *arXiv:1611.00036*  
 Diemand, J., Madau, P., & Moore, B. 2005, *MNRAS*, 364, 367  
 Eggen, O. J., Lynden-Bell, D., & Sandage, A. R. 1962, *ApJ*, 136, 748  
 Font, A. S., Johnston, K. V., Bullock, J. S., & Robertson, B. E. 2006, *ApJ*, 638, 585  
 Gaia Collaboration, Prusti, T., de Bruijne, J. H. J., et al. 2016, *A&A*, 595, A1  
 Gill, S. P. D., Knebe, A., & Gibson, B. K. 2004, *MNRAS*, 351, 399  
 Gilmore, G., Wyse, R. F. G., Norris, J. E., et al. 2012, *Msngr*, 147, 25  
 Gnedin, O. Y., Brown, W. R., Geller, M. J., & Kenyon, S. J. 2010, *ApJL*, 720, L108  
 Governato, F., Brook, C. B., Brooks, A. M., et al. 2009, *MNRAS*, 398, 312  
 Governato, F., Zolotov, A., Pontzen, A., et al. 2012, *MNRAS*, 422, 1231  
 Hattori, K., Valluri, M., Loebman, S. R., & Bell, E. F. 2017, *ApJ*, 841, 91  
 Hattori, K., Yoshii, Y., Beers, T. C., Carollo, D., & Lee, Y. S. 2013, *ApJL*, 763, L17  
 Jeans, J. H. 1915, *MNRAS*, 76, 70  
 Johnston, K. V., Bullock, J. S., Sharma, S., et al. 2008, *ApJ*, 689, 936  
 Kafle, P. R., Sharma, S., Lewis, G. F., & Bland-Hawthorn, J. 2012, *ApJ*, 761, 98  
 Katz, N., & White, S. D. M. 1993, *ApJ*, 412, 455  
 King, C., III, Brown, W. R., Geller, M. J., & Kenyon, S. J. 2015, *ApJ*, 813, 89  
 Knollmann, S. R., & Knebe, A. 2009, *ApJS*, 182, 608  
 Munn, J. A., Monet, D. G., Levine, S. E., et al. 2004, *AJ*, 127, 3034  
 Munshi, F., Governato, F., Brooks, A. M., et al. 2013, *ApJ*, 766, 56



- Pillepich, A., Madau, P., & Mayer, L. 2015, [ApJ](#), **799**, 184
- Rashkov, V., Pillepich, A., Deason, A. J., et al. 2013, [ApJL](#), **773**, L32
- Robertson, B., Bullock, J. S., Font, A. S., Johnston, K. V., & Hernquist, L. 2005, [ApJ](#), **632**, 872
- Sales, L. V., Navarro, J. F., Abadi, M. G., & Steinmetz, M. 2007, [MNRAS](#), **379**, 1464
- Santos-Santos, I. M., Brook, C. B., Stinson, G., et al. 2016, [MNRAS](#), **455**, 476
- Shen, S., Wadsley, J., & Stinson, G. 2010, [MNRAS](#), **407**, 1581
- Sirko, E., Goodman, J., Knapp, G. R., et al. 2004, [AJ](#), **127**, 914
- Smith, M. C., Evans, N. W., Belokurov, V., et al. 2009, [MNRAS](#), **399**, 1223
- Snaith, O. N., Bailin, J., Gibson, B. K., et al. 2016, [MNRAS](#), **456**, 3119
- Somerville, R. S., & Kolatt, T. S. 1999, [MNRAS](#), **305**, 1
- Spergel, D., Gehrels, N., Baltay, C., et al. 2015, [arXiv:1503.03757](#)
- Spergel, D. N., Verde, L., Peiris, H. V., et al. 2003, [ApJS](#), **148**, 175
- Stinson, G., Brook, C., Maccio, A. V., et al. 2013, [MNRAS](#), **428**, 129
- Stinson, G., Seth, A., Katz, N., et al. 2006, [MNRAS](#), **373**, 1074
- Tissera, P. B., Scannapieco, C., Beers, T. C., & Carollo, D. 2013, [MNRAS](#), **432**, 3391
- Valluri, M., Loebman, S. R., Bailin, J., et al. 2016, in IAU Symp. 317, The General Assembly of Galaxy Halos: Structure, Origin and Evolution, ed. A. Bragaglia et al. (Cambridge: Cambridge Univ. Press), 358
- Wadsley, J. W., Stadel, J., & Quinn, T. 2004, [NewA](#), **9**, 137
- Wang, W., Han, J., Cooper, A. P., et al. 2015, [MNRAS](#), **453**, 377
- Wilkinson, M. I., & Evans, N. W. 1999, [MNRAS](#), **310**, 645
- Williams, A. A., & Evans, N. W. 2015, [MNRAS](#), **454**, 698
- Xue, X.-X., Ma, Z., Rix, H.-W., et al. 2014, [ApJ](#), **784**, 170
- Xue, X.-X., Rix, H.-W., Yanny, B., et al. 2011, [ApJ](#), **738**, 79
- Xue, X. X., Rix, H. W., Zhao, G., et al. 2008, [ApJ](#), **684**, 1143
- Zolotov, A., Brooks, A. M., Willman, B., et al. 2012, [ApJ](#), **761**, 71
- Zolotov, A., Willman, B., Brooks, A. M., et al. 2009, [ApJ](#), **702**, 1058